Yao et al.

(E-mail: yaolu_cug@163.com)

Supplementary Information

This file provides supporting information for article "The crucial role of temperature in high-velocity weakening of faults: Experiments on gouge using host blocks with different thermal conductivities" by Yao et al. Topics covered here include:

1. Summary of experiments and supplementary data (Table DR1, Fig. DR1);
2. Details of temperature calculation (Table DR2, Fig. DR2);
3. Supplementary information on microstructures (Fig. DR3);
4. Details of fits to experimental data using a flash heating model updated by Platt et al., (2014) (Fig. DR4).

1. Summary of experiments and supplementary data

Two types of experiments were conducted in this study. We refer to the experiments with fixed slip rates (0.1-2.1 m/s) throughout the runs and with a constant slip rate of 1.9 m/s for 6.4 s followed by a linear deceleration within 24 s as standard constant-velocity tests and slow deceleration tests, respectively. For each experiment, 2.5 gram fault gouge was placed between the host blocks with the gouge layer thickness of ~ 1.2 mm. We ensured that the initial thickness/porosity of the gouge layer is consistent from test to test by compacting the gouge until the axial displacement stabilized before each experiment. The gouge material, host block, normal stress and slip rate for each experiment are given below (Table DR1). The peak friction coefficient (μ_p) for each test was obtained by reading the peak value from the friction curve. For standard constant-velocity experiments with dramatic weakening that can be described well by Mizoguchi's equation (Mizoguchi et al., 2007), the steady-state friction coefficient (μ_{ss}) and the slip-weakening distance (D_w) were determined by the least-square fitting with the equation. For standard constant-velocity tests with slight or without slip weakening, the μ_{ss} was obtained by averaging friction coefficient at and near the end of the test. We also corrected the extra torque resulting from the friction on the interface of the Teflon sleeve with the rotary host block. For the constant-velocity experiments with exponential-decay type slip weakening, the intercept method was used to correct the shear stress for Teflon friction (Togo et al., 2011; Yao et al., 2013a; using equivalent peak and steady-state shear stress of 0.091 MPa and 0.077 MPa). For the constant-velocity experiments with slight slip weakening and the slow deceleration tests, an averaged equivalent shear stress of 0.084 MPa was used to correct the shear stress for Teflon friction.

Table DR1: Summary of mechanical data from all experiments performed on the illite-quartz gouge and pure quartz gouge with four kinds of host blocks ("wall rocks") under room humidity. σ_n, V, μ_p, μ_{ss} and D_w denote normal stress, slip rate, peak friction coefficient, steady-state friction coefficient and slip-weakening distance, respectively.

Run number	Gouge material	Host block	σ_n (MPa)	V (m/s)	μ_p	μ_{ss}	D_w (m)
LHV610	Illite-quartz	Brass	1.0	0.1	0.82	0.75	/
LHV603	Illite-quartz	Brass	1.0	0.3	0.82	0.76	/
LHV346	Illite-quartz	Brass	1.0	0.5	0.81	0.65	/
LHV354	Illite-quartz	Brass	1.0	1.0	0.74	0.58	/
LHV596	Illite-quartz	Brass	1.0	1.0	0.81	0.62	/
LHV587	Illite-quartz	Brass	1.0	2.1	0.68	0.31	40.1
LHV601	Illite-quartz	Brass	1.0	1.9 + linear deceleration within 24s	0.74	/	/
LHV538	Quartz	Brass	1.0	1.0	0.77	0.61	/
LHV611	Illite-quartz	Stainless steel	1.0	0.1	/	0.77	/
LHV604	Illite-quartz	Stainless steel	1.0	0.3	0.80	0.69	/
LHV347	Illite-quartz	Stainless steel	1.0	0.5	0.71	0.52	/
LHV535	Illite-quartz	Stainless steel	1.0	1.0	0.67	0.28	27.5
LHV534	Illite-quartz	Stainless steel	1.0	2.1	0.65	0.21	16.0
LHV608	Illite-quartz	Stainless steel	1.0	1.9 + linear deceleration within 24s	0.72	/	/
LHV577	Quartz	Stainless steel	1.0	1.0	0.69	0.50	24.3
LHV607	Illite-quartz	Ti alloy	1.0	0.1	0.80	0.74	/
LHV606	Illite-quartz	Ti alloy	1.0	0.2	0.78	0.57	/
LHV605	Illite-quartz	Ti alloy	1.0	0.3	0.77	0.45	/
LHV517	Illite-quartz	Ti alloy	1.0	0.5	0.66	0.32	17.0
LHV513	Illite-quartz	Ti alloy	1.0	1.0	0.57	0.20	14.7
LHV516	Illite-quartz	Ti alloy	1.0	2.1	0.56	0.09	12.0
LHV609	Illite-quartz	Ti alloy	1.0	1.9 + linear deceleration within 24s	0.70	/	/
LHV602	Illite-quartz	Ti alloy	1.0	1.9 + linear deceleration within 24s	0.63	/	/
LHV576	Quartz	Ti alloy	1.0	1.0	0.64	0.46	14.6
LHV330	Illite-quartz	Gabbro	1.0	0.5	0.70	0.25	13.4
LHV355	Illite-quartz	Gabbro	1.0	1.0	0.62	0.17	7.5
LHV339	Illite-quartz	Gabbro	1.0	2.1	0.63	0.10	5.8
LHV578	Quartz	Gabbro	1.0	1.0	0.67	0.27	16.9

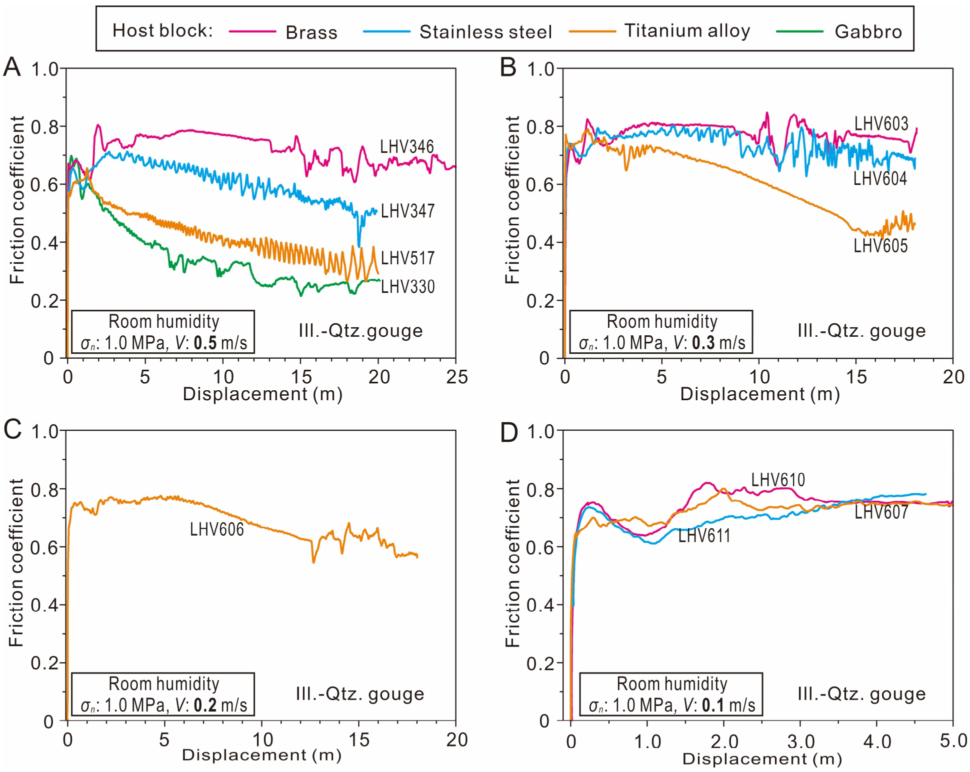

Figure DR1: Friction coefficient versus displacement for the standard constant-velocity experiments conducted on the illite-quartz gouge at a normal stress of 1.0 MPa and various slip rates of 0.5 m/s (A), 0.3 m/s (B), 0.2 m/s (C) and 0.1 m/s (D) under room humidity, using host blocks made of brass, stainless steel, titanium alloy and gabbro.

2. Details of temperature calculation

Temperature rise during the experiment was calculated with the finite element method using COMSOL software. The geometric model in the calculation was built according to the sample assembly with real sizes of host blocks, Teflon sleeve and gouge layer (~1.2 mm thick). We are mainly concerned with how the thermal conductivity of the host blocks influences the temperature rise, so the main variable physical properties are listed in Table DR2 below and other properties follow those used in Yao et al. (2013b).

Boundary and initial conditions were set according to the real situations in the experiments as specified in Yao et al. (2013b). The main heat source is assumed to be the measured shear stress, and the friction on the interface of the Teflon sleeve and moving host block was set as a secondary heat source. However, the distribution of heat source (or velocity) in the gouge layer was set based on microstructural observations. For the illite-quartz gouge, the shear deformation is localized in two main boundary-parallel shear zones that are each ~100 μm thick and adjacent to the moving and stationary host blocks, respectively (Fig.3 and Fig. DR3 A-B). Accordingly, we assume that relative slip only occurs in these two shear zones with relative slip velocity equaling to half of the target slip rate of the experiment. In contrast, for the pure quartz gouge, the shear deformation seems to distribute in the entire gouge layer without clear shear zones (Fig. DR3 C-D; see changes in grain shape of quartz), thus the heat source was assumed to be a distributed shear case. The energy consumed in the dehydroxylation reaction of illite was ignored in the temperature calculation for the illite-quartz gouge, since the enthalpy of dehydration/dehydroxylation reaction of common clay minerals (e.g. smectite and illite) are only a few percent of the frictional work in common high-velocity friction experiments (Kitajima et al., 2010; Hirono et al., 2013). The calculation was validated by the temperature measured with thermocouples at two or three positions on the interface of the gouge layer and stationary host block (see an example in Fig. DR2).

For solid-cylindrical specimens, 87.5% of torque is exerted from the friction on the outer half of the simulated fault if the friction is considered uniform. Temperature rise is notable in the outer half of the gouge layer, but is much gentler for the inner half. Thus, we use an averaged temperature for the outer half of the shear zone to analyze the temperature dependence of the high-velocity friction and the dominant weakening mechanisms in the article.

Table DR2: A list of thermal conductivity (*K*), specific heat capacity (C_p), density (ρ) of the four kinds of host blocks and mineral grains used in the temperature calculation.

Materials	K (W/m/k)	C_p (J/kg/k)	ρ (kg/m^3)	Reference
Brass (C28000)	123	376	8390	Cverna (2002)
Stainless steel (AISI 316)	15	500	7980	Cverna (2002)
Titanium alloy (Ti90Al6V4)	5.8	580	4420	Online data [a], Cverna (2002)
Shanxi Gabbro	3.25	650	3200	Yao et al., (2013b), Waples and Waples (2004)
Illite	1.9	900	2700	Brigaud and Vasseur, (1989), Skauge et al., (1983)
Quartz	7.7	740	2700	Clauser and Huenges, (1995), Waples and Waples (2004)

1. [a] Website of Goodfellow Cambridge Ltd., http://www.goodfellow.com/E/Titanium-Aluminium-Vanadium.html.

2. Properties of Teflon sleeve, loading column and specimen holder follow those used in Yao et al. (2013b).

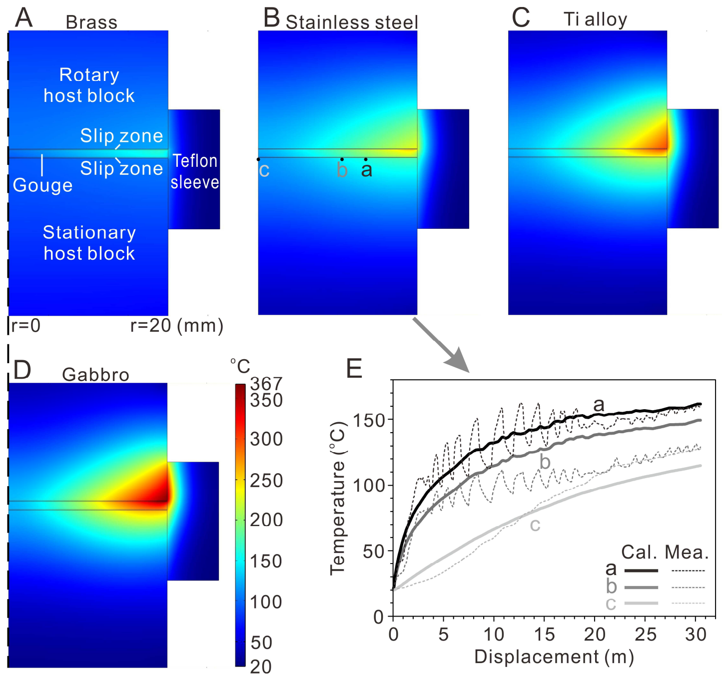

Figure DR2: A-D: Calculated temperature distribution at the end of experiments on the illite-quartz gouge deformed with host blocks made of brass (A), stainless steel (B), Titanium alloy (C) and gabbro (D), respectively, at a slip rate of 1.0 m/s and a normal stress of 1.0 MPa (runs LHV354, LHV535, LHV513 and LHV355, respectively). E: Comparison of calculated (solid curves) and measured (dashed curves) temperatures for the test shown in Fig. DR2 B at three locations (a, b and c) on the interface of gouge and stationary host block.

Temperature was measured with K-type thermocouples of 1.6 mm in diameter that inserted into small holes in the stationary host specimens and fixed on the gouge-rock interface by high-temperature cement. Reasonable agreement was found between the measured and calculated temperature data although the measured data sometimes show complex oscillations.

3. Supplementary information on microstructure

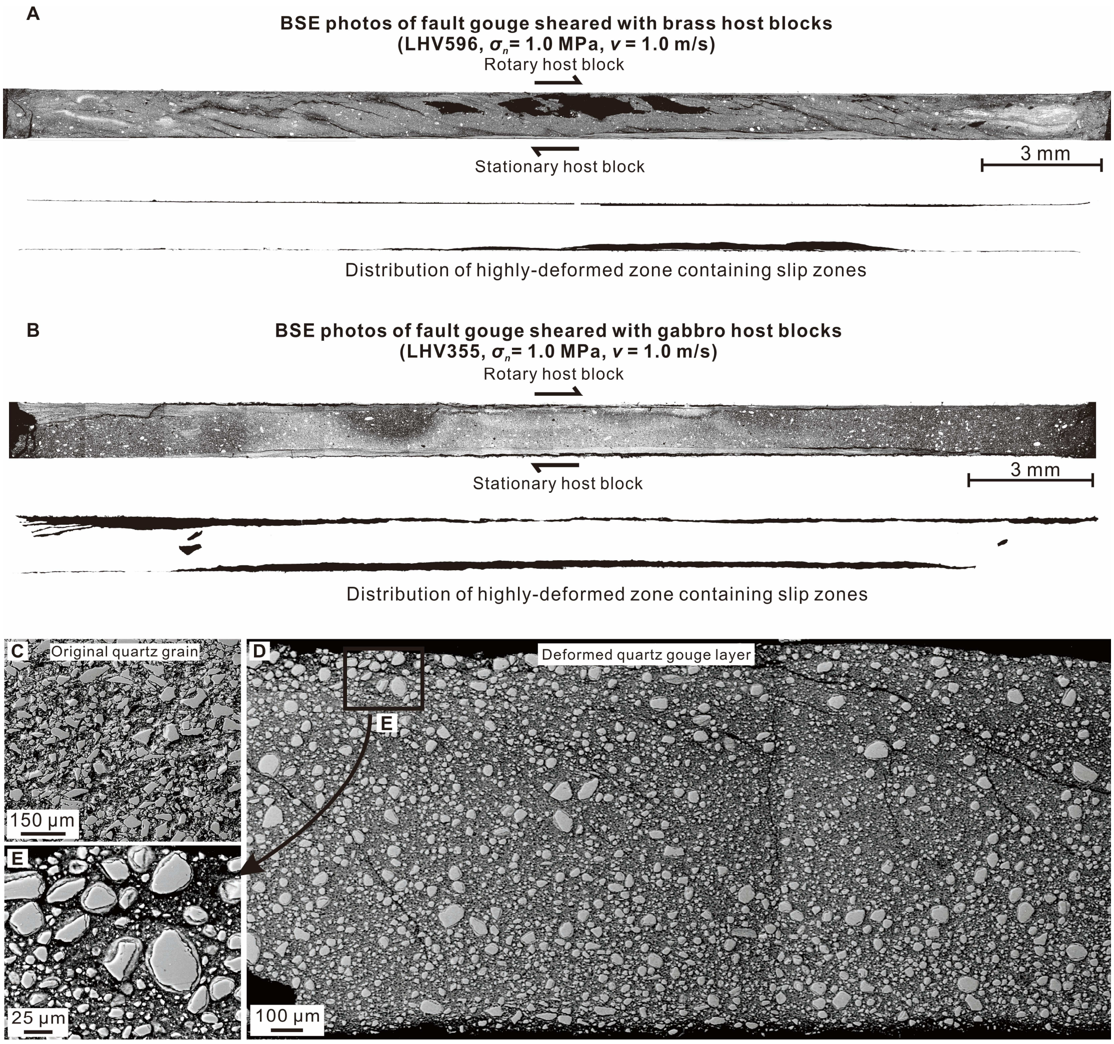

Figure DR3: A-B: Back-scattered electron (BSE) images of the deformed illite-quartz gouge layer and simple schematic sketches highlighting the highly-deformed zones. The gouge samples were deformed with brass (A) and gabbro (B) host blocks under a slip rate V of 1.0 m/s and a normal stress σ_n of 1.0 MPa. In both cases, double highly-sheared zones of tens of to about 100 microns in thickness were developed near the rotary and stationary host blocks, respectively. C-E: Comparison of original quartz grains and deformed quartz gouge layer (after run LHV538, σ_n = 1.0 MPa, V =1.0 m/s). Most of the quartz grains are deformed and grain sizes reduce, suggesting fairly distributed shear deformation. Close-up images reveal that the quartz grains change their shapes from angular grains to nearly round ones (see C-D) with structures look similar to clay-clast aggregates (CCAs; Boutareaud et al. 2008, 2010; see E). The formation of CCAs and their implications have been debated in recent years (Han et al., 2012; Rempe et al., 2014). Our experiments suggest that the formation of CCAs is not necessarily related to the dynamic weakening process, since almost no slip weakening was observed in the experiment (with brass host blocks) that develop CCAs structures as shown in D-E.

4. Details of fits to experimental data using a flash heating model updated by Platt et al., (2014)

The classic model of flash heating gives a characteristic weakening velocity V_w (Rice 2006), above which the dynamic weakening occurs due to thermal degradation of the strength of asperity contacts:

$$V_w = \frac{\pi\alpha}{D}\left[\frac{\rho c\left(T_w - T_f\right)}{\tau_c}\right]^2 \quad \text{(Eq. 1)},$$

where α is the thermal diffusivity, ρ is the density, c is the heat capacity, D is asperity size, T_w is the weakening temperature, T_f is the ambient temperature of the fault surface, and τ_c is the contact shear strength.

For $V<V_w$, the friction coefficient is a constant value equal to the coefficient at low slip rates f_0, while for $V>V_w$

$$f(V) = (f_0 - f_w)\frac{V_w}{V} + f_w \quad \text{(Eq. 2)},$$

where f_w is the friction coefficient in the weakened state.

Using the flash heating models developed in Rice (2006) and Beeler et al. (2008), Platt et al. (2014) showed that temperature effects could be important, leading to large drops in V_w as the fault temperature evolves in the deforming gouge. Thus Eq.2 predicts a slip weakening process as V_w reducing with increasing displacement even at a constant slip rate V. If we neglect the dynamic changes of material properties in the short experimental period following former published work (e.g. Goldsby and Tullis, 2011), the properties such as α, ρ, c, D and τ_c all collapse into a constant term. This term along with T_w and the initial value of T_f determines the initial weakening velocity V_{w_init} at the onset of the experiment (i.e. the V_w in the classic flash heating model). In summary, with measured friction coefficient and calculated temperature versus displacement d, we can get three meaningful independent parameters in the fitting, i.e. T_w, f_w and V_{w_init}, using the following rearranged equation:

$$f\left(V, T_f, d\right) = (f_0 - f_w)\frac{(T_w - T_f(d))^2}{V}\frac{V_{w\_init}}{(T_w - T_f|_{d=0})^2} + f_w \quad \text{(Eq. 3)}.$$

The volume-averaged temperature of outer-half slip zone is taken as T_f in the fitting (see details in section 2 in the Data Repository). The friction coefficient at low slip rates f_0 is assumed to be the peak friction coefficient in the experiments, which is slightly different from run to run. The ratio of the two square terms in Eq.3 predicts how V_w evolves with T_f and d as compared to its initial value at the beginning of the experiment,

$$V_w(T_f) = \frac{(T_w - T_f(d))^2}{(T_w - T_f|_{d=0})^2} V_{w\_init} \quad \text{(Eq. 4)}.$$

In Fig. 4B-C in the main text, the fits to the five experiments of the illite-quartz gouge were obtained by using same V_{w_init}, T_w and f_w, since we think these three parameters should be inherent properties of the gouge material. However, we cannot get exactly the same values of V_{w_init}, T_w and f_w by fitting each experiment separately because of the uncertainties in the experiments (e.g. the initial compaction and Teflon friction, etc.) and in the temperature calculation (e.g. the thickness of the slip zone and the variation in slip rate within the gouge layer). Fig. DR4 A-B shows how the standard deviation varies with the two fitting parameters (T_w and V_{w_init}) in the case of using optimal f_w for two representative experiments on the illite-quartz gouge (runs LHV513 and LHV609). Note that the trade-off between T_w and V_{w_init} allows a range of values to provide a reasonable fit to the experimental data. Considering the effects of f_w, the tradeoffs among the three parameters are actually much more complex than what we show here. The red and green stars in Fig. DR4 A-B indicate the locations of the best fitting parameters obtained from the individual fit to the single test and the multiple fits to all the nine tests with dramatic slip weakening, respectively. As shown in Fig. DR4 D-E, the deviation between measured data and theoretical prediction is smaller in the individual fit (see red curves). But in order to have clearer physical meanings, we adopt the fitting parameters obtained from the multiple fits although the deviation is larger in this case.

As a comparison, the fitting results for the quartz gouge data are shown in Fig. DR4 C and F although the only one experiment (LHV578) showing dramatic weakening was involved in the fitting. In consideration of the parameter tradeoffs and the relatively high μ_{ss} in run LHV578 (0.27; it can be much lower at higher velocities), we simply use fixed f_w of 0, 0.04 (quartzite data from Goldsby and Tullis, 2011), 0.1 and 0.15, and find optimal T_w and V_{w_init} through fitting. As is shown in Fig. DR4 F, the fitting curves almost overlap but the fitted parameters vary a lot, probably implying large uncertainties in the fitting due to limited experimental data for the quartz gouge.

The fits to the illite-quartz gouge data yield T_w = 296 °C, V_{w_init} = 2.31 m/s, and f_w = 0.15. We think the estimated T_w of 296 °C for the illite-quartz gouge is reasonable if we consider that the breakdown of illite can weaken the asperity contacts in the illite-quartz mixture. Hirono et al. (2013) reported thermogravimetric analysis results of experimentally sheared illite. They found that the dehydroxylation (breakdown of illite crystal structure) temperature of the sheared illite can be lowered to 200~300 °C, as compared to over ~400°C for the undeformed illite. In consideration of the uncertainties in reaction kinetics during high-speed frictional sliding, the T_w of 296 °C for the illite-quartz gouge is reasonable with respect to the physical expectation.

The fits to quartz gouge data yield T_w = 650-850 °C and V_{w_init} = 1.94–2.63 m/s in the case of fixing f_w = 0–0.15. The estimated T_w of ~650–850 °C may be linked to a phase transition. This temperature is much lower than bulk melting temperature of quartz, but previous work has claimed that a layer of melt may not be required for weakening by flash heating (Molinari et al., 1999; Rice, 2006). Furthermore, even assuming that the flash weakening is due to melting on contacts, it does not mean that the T_w has to be equal to the bulk melting temperature determined from lab measurement. One important reason is that melting is a physico-chemical process related to thermodynamics, so the high-rate shear deformation along with frictional heating in our experiments probably can enhance the kinetics of melting on asperity contacts and thus lower the melting point.

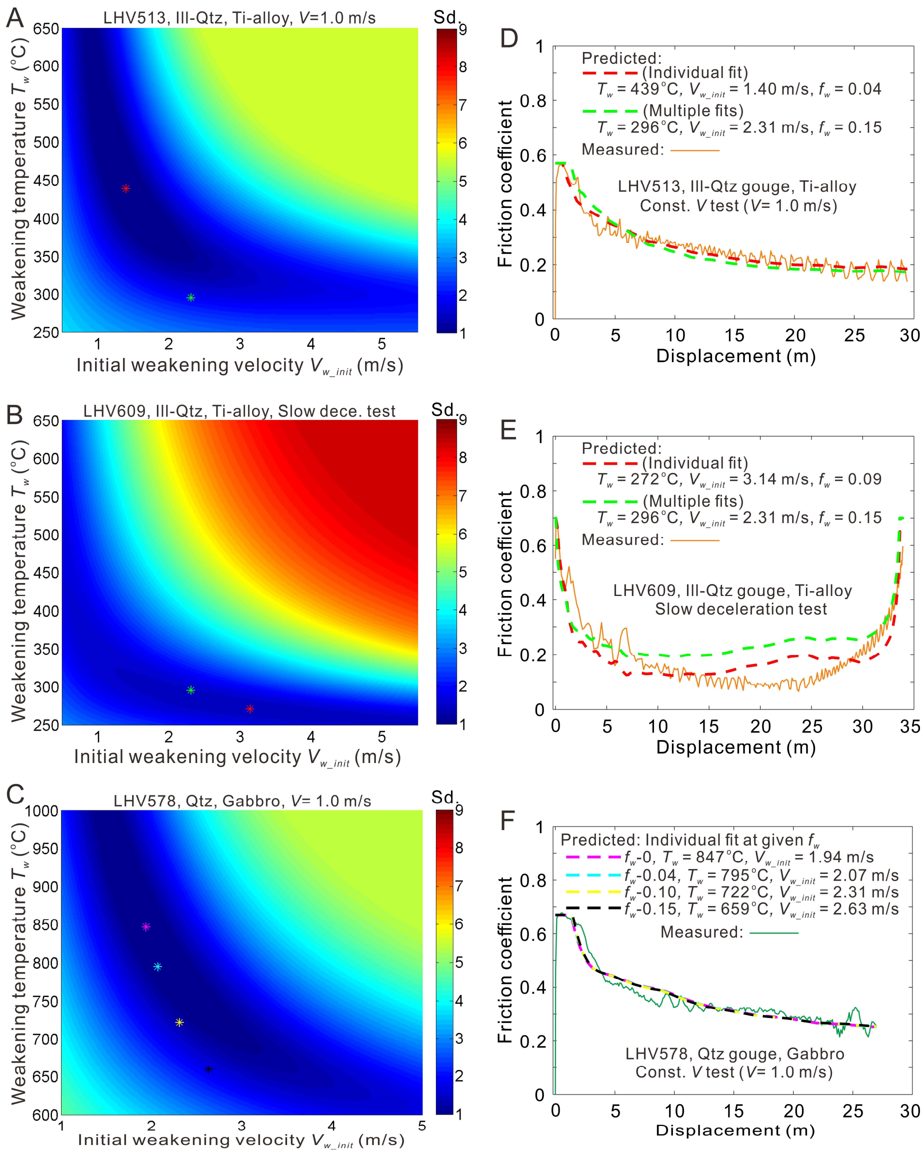

Figure DR4: A-C: The standard deviation (Sd.) of the fits plotted as a function of weakening temperature T_w and initial weakening velocity V_{w_init} for two representative tests on the illite-quartz gouge using Ti-alloy host blocks (A-B) and one test on the quartz gouge using gabbro host blocks (C). D-E: Comparison of measured frictional data (solid orange curves) and predicted friction evolutions using the fitting parameters

(T_w, f_w and V_{w_init}) obtained from the individual fit to the single test (dashed red curves) and the multiple fits to all the nine tests showing dramatic slip weakening (μ_{ss} less than ~0.3; LHV330, LHV535, LHV513, LHV355, LHV534, LHV516, LHV339, LHV608 and LHV609; dashed green curves). F: Comparison of the measured quartz gouge data and the model predictions obtained from individual fit, with given f_w of 0, 0.04, 0.1 and 0.15. The stars in A-C indicate the locations of the fitted T_w and V_{w_init} corresponding to the fitted curves shown in D-F, respectively.

References Cited

Beeler, M., T. Tullis and D. Goldsby (2008), Constitutive relationships and physical basis of fault strength due to flash heating, *J. Geophys. Res.*, 113, B01401, doi: 10.1029/2007JB004988.

Boutareaud, S., D.-G. Calugaru, R. Han, O. Fabbri, K. Mizoguchi, A. Tsutsumi, and T. Shimamoto (2008), Clay-clast aggregates: A new textural evidence for seismic fault sliding?, Geophys. Res. Lett., 35(5), L05302, doi: 10.1029/2007gl032554.

Boutareaud, S., A.-M. Boullier, M. Andréani, D.-G. Calugaru, P. Beck, S.-R. Song, and T. Shimamoto (2010), Clay clast aggregates in gouges: New textural evidence for seismic faulting, J. Geophys. Res., 115(B02408), doi: 10.1029/2008jb006254.

Brigaud, F., and G. Vasseur (1989), Mineralogy, porosity and fluid control on thermal conductivity of sedimentary rocks, *Geophy. J. Int.*, *98*(3), 525-542.

Clauser, C. and E. Huenges (1995). Thermal conductivity of rocks and minerals. *Rock physics and phase relations: a handbook of physical constants 3*: 105-126.

Cverna, F., 2002, ASM ready reference: thermal properties of metals: USA, ASM International, 560 p.

Goldsby, D. L., and T. E. Tullis, 2011, Flash heating leads to low frictional strength of crustal rocks at earthquake slip rates: *Science*, 334, 216-218. doi:10.1126 /science.1207902.

Han, R., and T. Hirose (2012), Clay–clast aggregates in fault gouge: An unequivocal indicator of seismic faulting at shallow depths?, J. Struct. Geol., 43, 92-99, doi: 10.1016/j.jsg.2012.07.008.

Hirono, T., W. Tanikawa, G. Honda, J. Kameda, J. Fukuda, and T. Ishikawa, 2013, Importance of mechanochemical effects on fault slip behavior during earthquakes: *Geophys. Res. Lett.*, 40, 2988–2992, doi:10.1002/grl.50609.

Kitajima, H., J. S. Chester, F.M. Chester, and T. Shimamoto (2010), High-speed friction of disaggregated ultracataclasite in rotary shear: Characterization of frictional heating, mechanical behavior, and microstructure evolution, *J. Geophys. Res.*, 115, B08408, doi:10.1029/2009JB007038.

Mizoguchi, K., T. Hirose, T. Shimamoto, and E. Fukuyama (2007), Reconstruction of seismic faulting by high-velocity friction experiments: An example of the 1995 Kobe earthquake, *Geophys. Res. Lett.*, 34(L01308), doi: 10.1029/2006gl027931.

Molinari, A., Estrin, Y., Mercier, S., 1999. Dependence of the Coefficient of Friction on the Sliding Conditions in the High Velocity Range. J. Tribol. 121, 35-41, doi: 10.1115/1.2833808.

Platt J., B. Proctor, T. Mitchell, G. Hirth, D. Goldsby, G. Di Toro, N. Beeler, T. Tullis, 2014, The role of gouge and temperature on flash heating and its hysteresis: American Geophysical Union, Fall Annual Meeting, abs. S11C-4360.

Rempe, M., S. A. F. Smith, F. Ferri, T. M. Mitchell, and G. Di Toro (2014), Clast-cortex aggregates in experimental and natural calcite-bearing fault zones, J. Struct. Geol., 68, Part A(0), 142-157, doi: http://dx.doi.org/10.1016/j.jsg.2014. 09.007.

Rice, J. R., 2006, Heating and weakening of faults during earthquake slip *J. Geophys. Res.*, 111, B05311, doi: 10.1029/2005JB004006.

Skauge, A., N. Fuller, and L. G. Hepler (1983), Specific heats of clay minerals: Sodium and calcium kaolinites, sodium and calcium montmorillonites, illite, and attapulgite, *Thermochim. Acta*, *61*(1–2), 139-145.

Togo, T., T. Shimamoto, S. Ma, and T. Hirose (2011), High-velocity frictional behavior of Longmenshan fault gouge from Hongkou outcrop and its implications for dynamic weakening of fault during the 2008 Wenchuan earthquake, Earthquake Sci., 24(3), 267-281, doi: 10.1007/s11589-011-0790-6.

Waples, D. W., and J. S. Waples (2004), A review and evaluation of specific heat capacities of rocks, minerals, and subsurface fluids. Part 1: Minerals and nonporous rocks, *Nat. Resour. Res.*, *13*(2), 97-122.

Yao, L., S. Ma, T. Shimamoto, and T. Togo (2013a), Structures and high-velocity frictional properties of the Pingxi fault zone in the Longmenshan fault system, Sichuan, China, activated during the 2008 Wenchuan earthquake, *Tectonophysics*, 599, 135–156, http://dx.doi.org/10.1016/j.tecto.2013.04.011.

Yao, L., T. Shimamoto, S. Ma, R. Han, and K. Mizoguchi (2013b), Rapid postseismic strength recovery of Pingxi fault gouge from the Longmenshan fault system: Experiments and implications for the mechanisms of high-velocity weakening of faults, *J. Geophys. Res.*, *118*(8), 4547-4563, doi:10.1002/jgrb.50308.